

Supplementary Materials for
**Topology optimization and 3D printing of multimaterial
magnetic actuators and displays**

Subramanian Sundaram*, Melina Skouras, David S. Kim, Louise van den Heuvel, Wojciech Matusik

*Corresponding author. Email: subras@csail.mit.edu

Published 12 July 2019, *Sci. Adv.* **5**, eaaw1160 (2019)

DOI: 10.1126/sciadv.aaw1160

The PDF file includes:

- Fig. S1. Material characteristics.
- Fig. S2. Experimental verification of tilting angles.
- Fig. S3. Two-axis tilting panels.
- Fig. S4. Dynamic mechanical analysis of the elastic material family used in the soft torsional hinges.
- Fig. S5. Large-amplitude bandwidth measurements.
- Fig. S6. Actuator long-term cycling.
- Fig. S7. Experimental setup for dynamic actuation.
- Fig. S8. 3D-printed water lily design.
- Fig. S9. Spike actuator arrays design.
- Fig. S10. Dot gain images.
- Fig. S11. Topology optimization—Optical and mechanical properties.
- Fig. S12. Measurement setup for characterizing the Van Gogh actuator.
- Fig. S13. Modeling of the external magnetic field.
- Legends for movies S1 to S4

Other Supplementary Material for this manuscript includes the following:

(available at advances.sciencemag.org/cgi/content/full/5/7/eaaw1160/DC1)

- Movie S1 (.mp4 format). Video showing the dynamic actuation of the reflective panel array used to raster the MIT logo.
- Movie S2 (.mp4 format). The printed water lily is placed at fluid interfaces and actuated using a permanent magnet.
- Movie S3 (.mp4 format). Actuation of panel actuators at different frequencies for bandwidth measurements and long-term actuation (1000 cycles).
- Movie S4 (.mp4 format). Topology optimization of actuators.

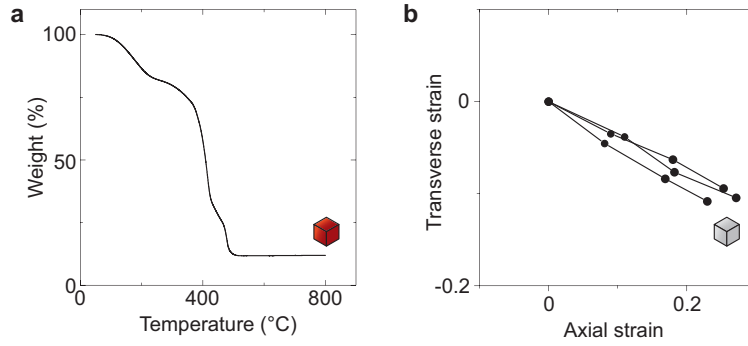


Fig. S1. Material characteristics. A. Thermogravimetry measurements of the MPC shows $\sim 12\%$ nanoparticle loading B. Poisson's ratio measurement for the elastic polymer (ELA).

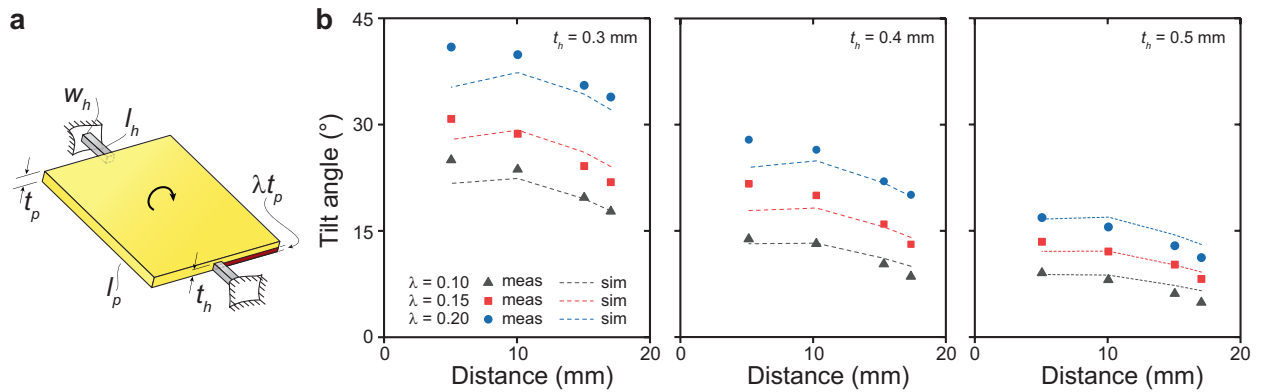


Fig. S2. Experimental verification of tilting angles. A. A single panel actuator was designed with magnetic material on one half of the panel for a fraction of the thickness λ . To verify the tilting angle as a function of geometric design changes, the fraction λ and thickness of the hinge, t_h , were varied. B. Experimental measurements of tilting angles are shown as a function of the distance from the permanent magnet, along with the results of simulations using our soft-joint solver. It can be seen that as the ratio of the magnetic material thickness, λ is increased, the tilting angle scales nearly linearly with it. Further, as expected the angle of tilting reduces with the thickness of the hinge (torsional stiffness of the ELA hinge).

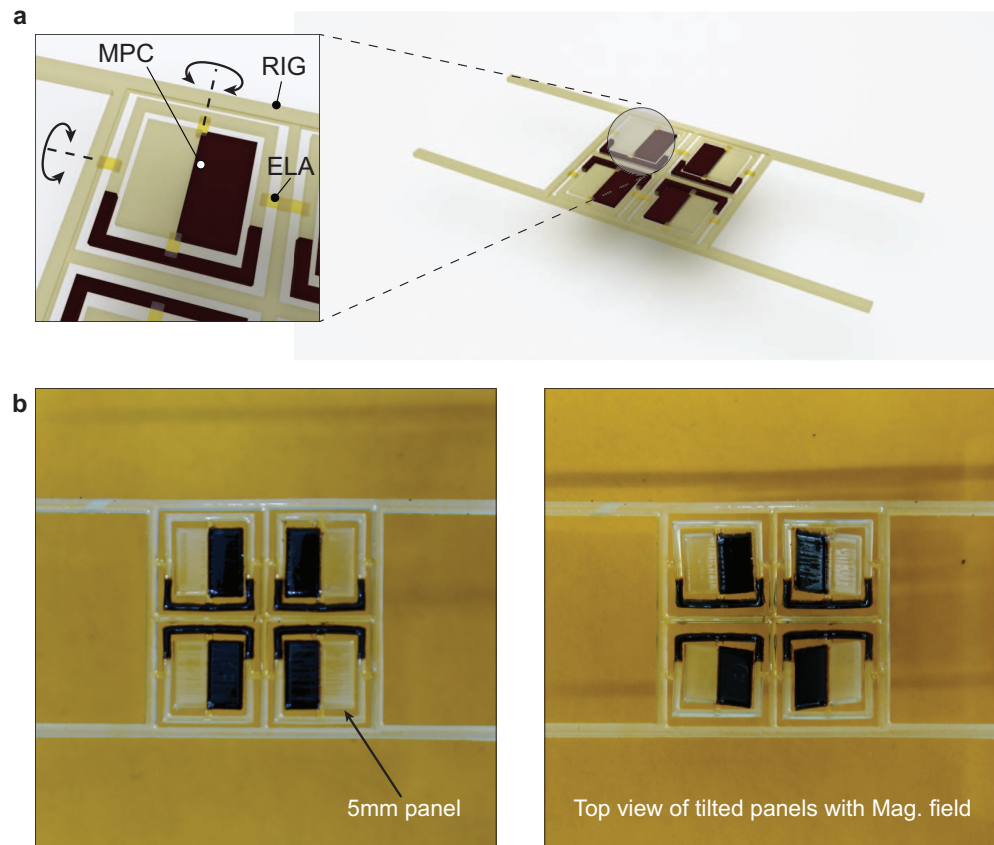


Fig. S3. Two-axis tilting panels. A. Scaled rendering of the 2×2 array of panels shows the three materials used in the design. The hinges (0.5 mm long) are made out of the elastic polymer (ELA), while each 5 mm panel is split equally into regions with MPC and the clear rigid material (RIG). Each panel is held by another frame that can itself tilt in an orthogonal direction. B. Top-view images of the printed part without and with an applied magnetic field (see Materials and Methods).

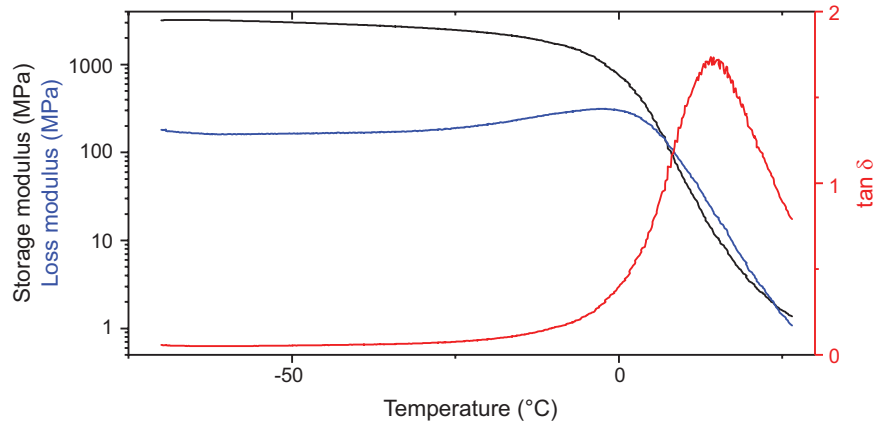


Fig. S4. Dynamic mechanical analysis (DMA) of the elastic material family used in the soft torsional hinges. Measured storage and loss modulus of the elastic material family cycled at 1 Hz in the linear regime using DMA. It can be seen that the measured $\tan \delta$ is ~ 1 at room temperature which corresponds with the damped response of the actuators at room temperature.

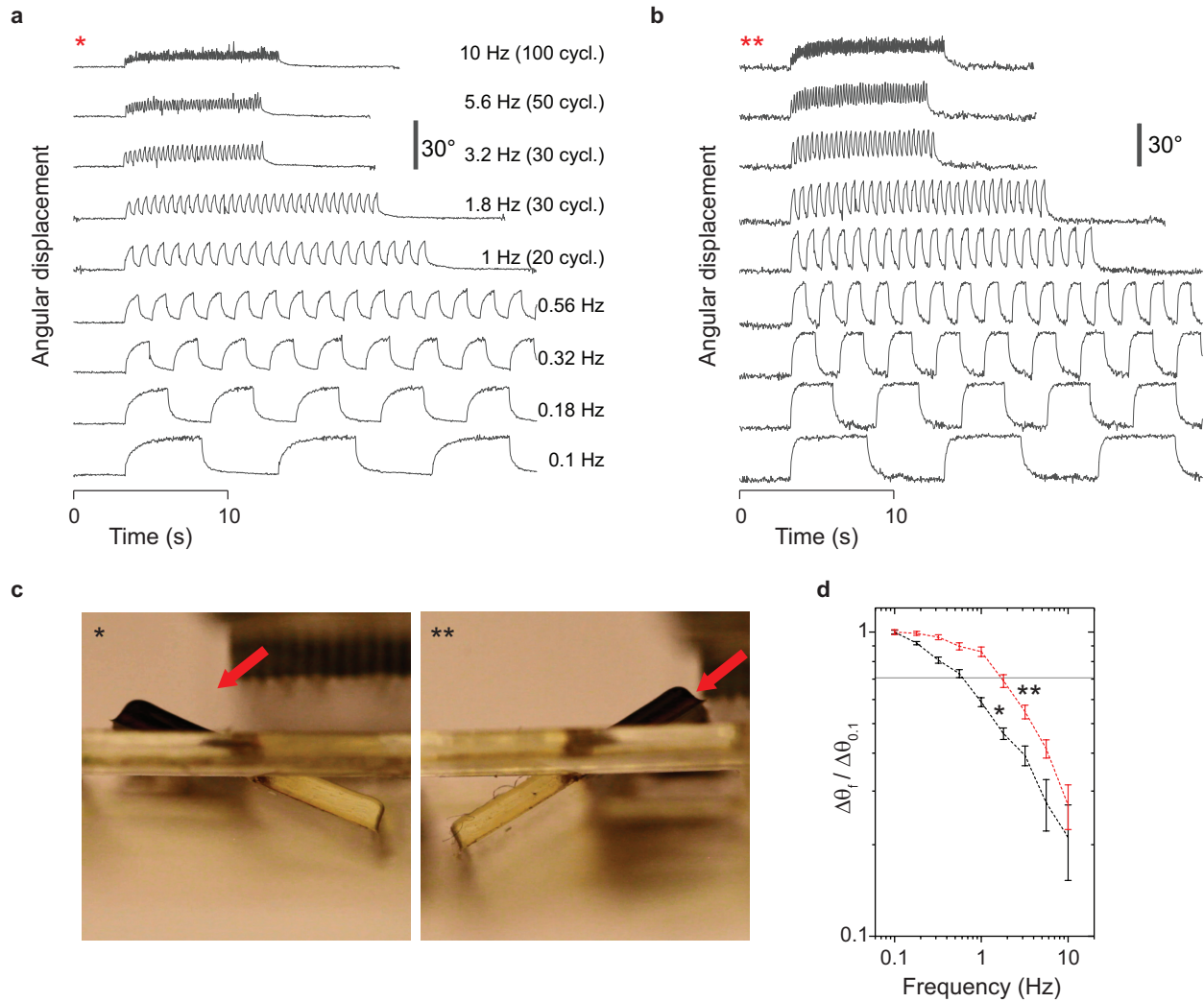


Fig. S5. Large-amplitude bandwidth measurements. A. and B. show the measured angular displacement of the panel actuator designs described in Fig. 3A when actuated in the large amplitude regime. In 'A' the actuator is oriented such the actuator experiences an increasing force with displacement (*). In the other case (**), the actuator has a stable displacement when the panel aligns with the direction of the maximum gradient of the magnetic field (near the corner). C. Images corresponding to * and ** respectively (see movie S3). The red arrow shows the corner of the electromagnet (steepest gradient). D. Normalized angular displacement amplitude shows that the apparent bandwidth in large amplitude actuation can be high depending on the magnetic field landscape (identical to Fig. 3F).

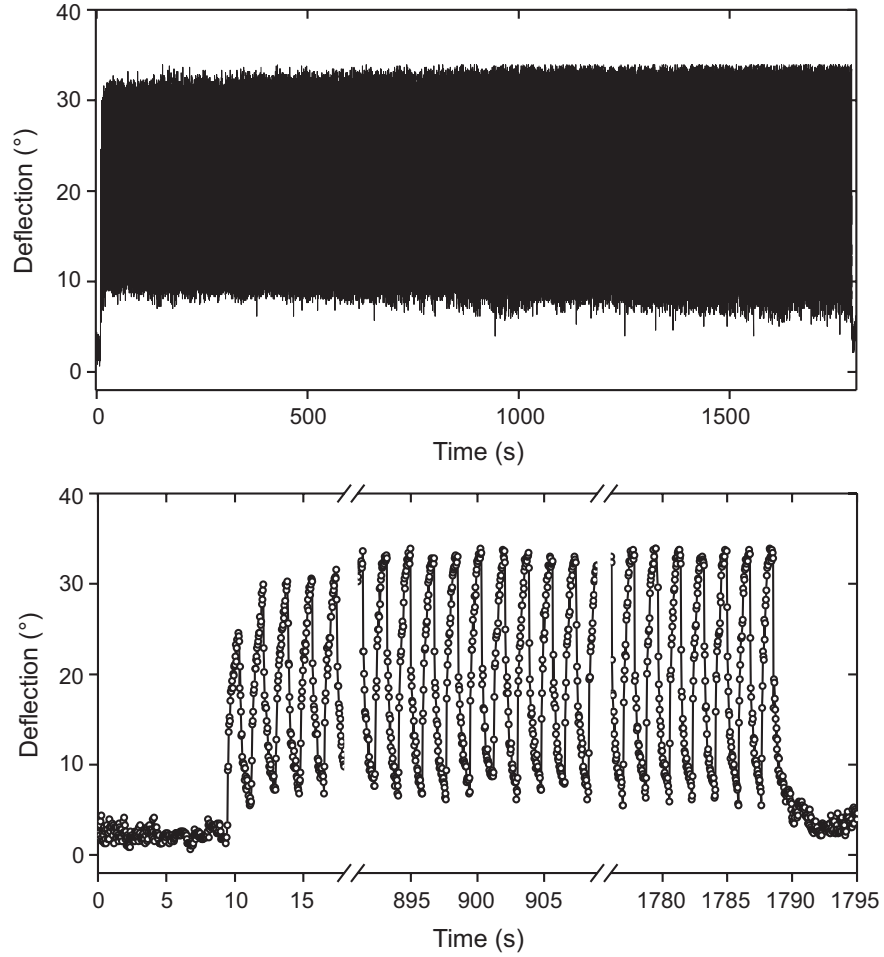


Fig. S6. Actuator long-term cycling. Plot shows the measured deflection of the actuator design in Fig. 3A for 1000 actuation cycles at 0.56 Hz (~ 30 minutes). The bottom plot shows the deflection over the first and last few cycles. There is no visible degradation after 1000 cycles (see movie S3).

Dynamic actuation to raster images

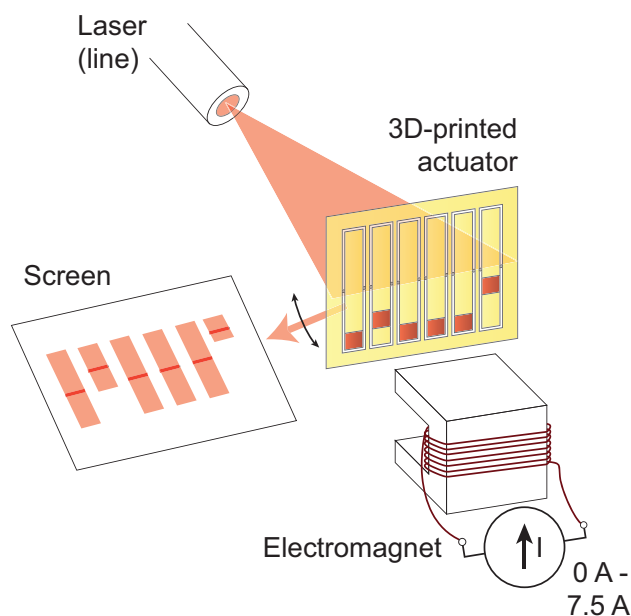


Fig. S7. Experimental setup for dynamic actuation. A 6-element array of mirrors is fabricated by 3D-printing all the materials on top of a polyimide film coated with a thin layer of silver nanoparticles. On removing the part from the polyimide film (and etching the freely exposed silver layers) the lower surface of the part attains a mirror-like surface finish. The printed sample is shown in Fig. 4B. The setup shows a line laser that is focused on the printed actuator array that is placed in front of an electromagnet. The laser line is reflected by the shiny surface of the actuator onto the screen. The deflection of the mirrors are controlled by the current through the electromagnet (0 A - 7.5 A).

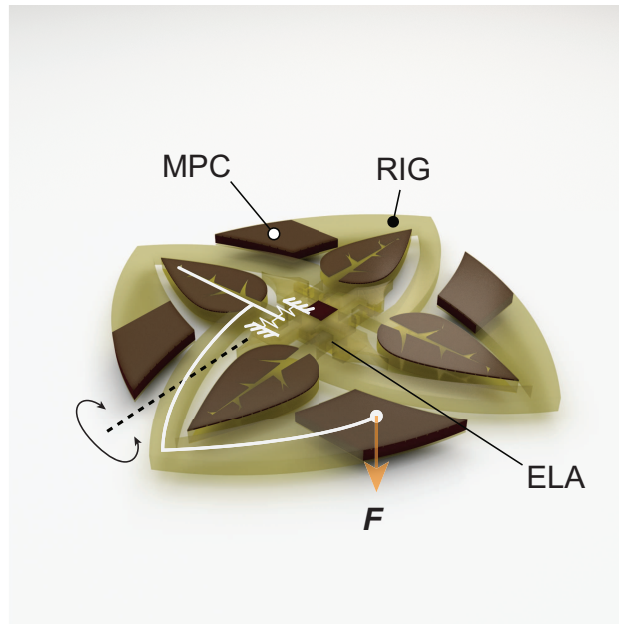


Fig. S8. 3D-printed water lily design. The rigid frame of each petal is shown in white, overlaid on one panel of the rendering. Typically 2 - 5 layers of the MPC ink are used to design the petal pattern. Each petal is attached to two torsional springs made with ELA. The torque to lift the petal is generated by an island of magnetic material attached to a long curved arm.

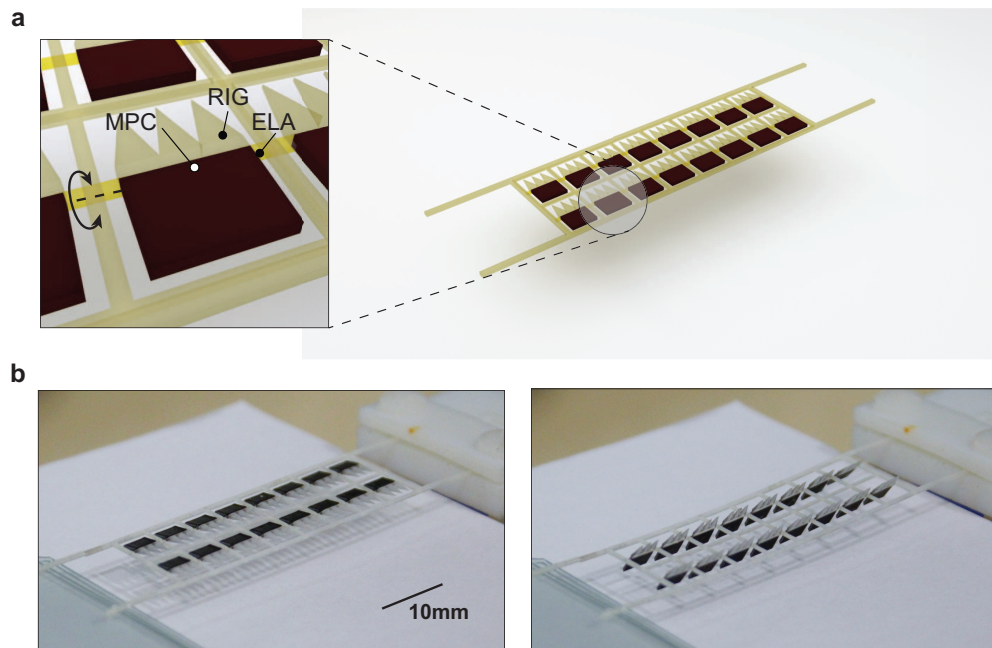


Fig. S9. Spike actuator arrays design. A. Rendering of the actuator array showing the ELA, RIG and MPC regions. B. Panels tilt uniformly on the application of a magnetic field. Here the magnet is held ~ 5 mm from the printed part, closer than the typical distance of 1 cm.

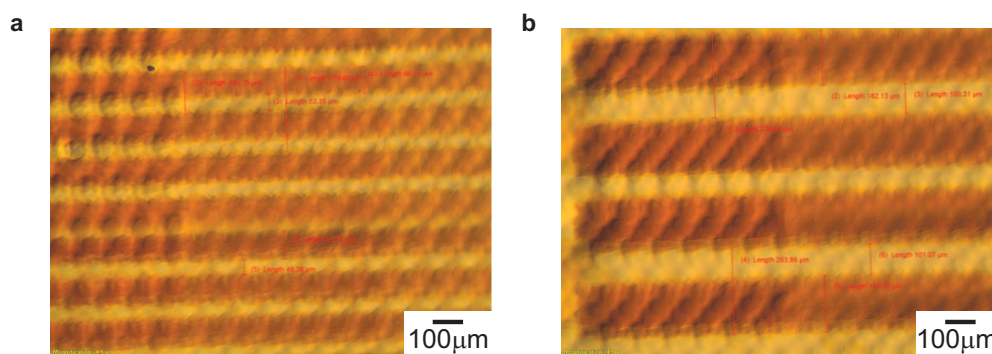


Fig. S10. Dot gain images. A. 2-voxel wide stripes and B. 4-voxel wide stripes. Dark stripes are the cured MPC ink and the lighter stripes are the cured RIG ink.

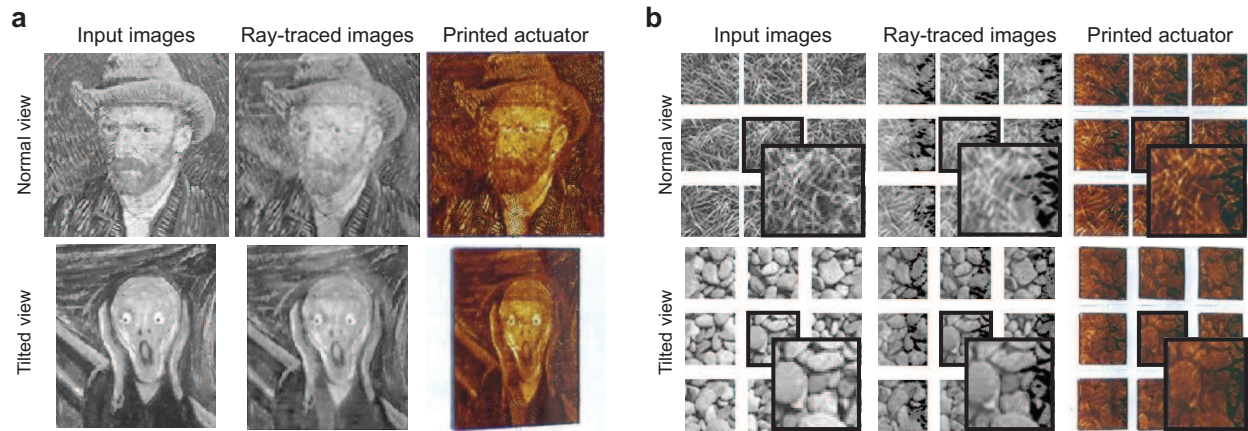


Fig. S11. Topology optimization—Optical and mechanical properties. Left: ‘Self portrait with Grey Felt Hat’, van Gogh. Image from public domain. Right: from (63). Image used with permission. Given a pair of target grayscale images corresponding to desired top views of the panel array at two different tilting angles (here, 0° and 30°), our topology optimization framework optimizes the material distribution such that they tilt to the right angles and their appearances matches the target images. Photographs of the 3D-printed panels under no external magnetic field (top) and under an external magnetic field (bottom) are shown on the right. (A) and (B) show results for the “Van Gogh” - “Scream” and the 3×3 grass-stones texture optimization respectively.

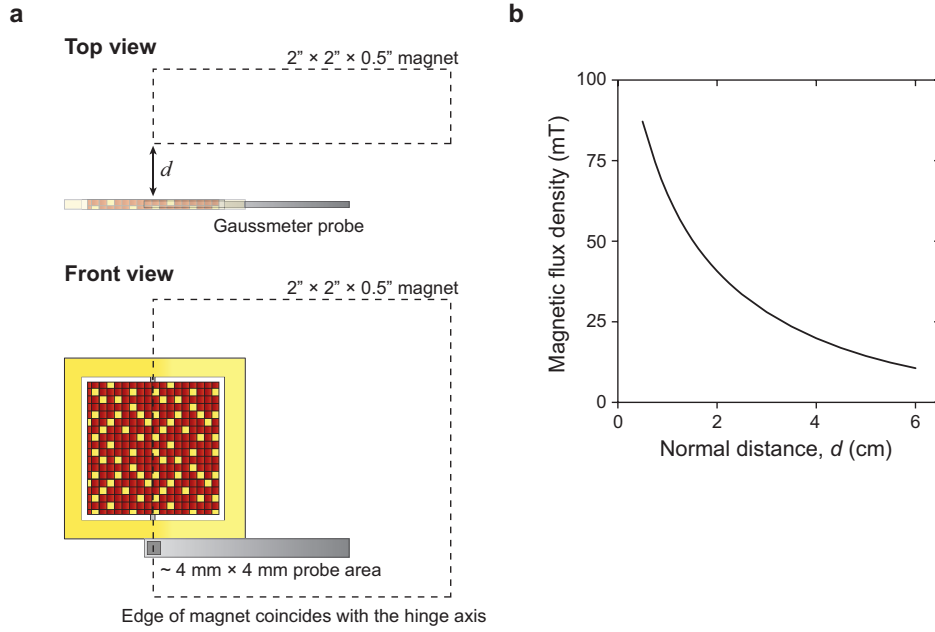


Fig. S12. Measurement setup for characterizing the Van Gogh actuator (Images in Fig. 6 and characteristics in Fig. 7A, 7B). A. To ensure that the topology optimized actuator tilts one way consistently, the magnet was positioned with an offset such that the edge of the magnet coincides with the hinge axis as shown in the setup. The magnetic field was measured using the gaussmeter probe positioned in the same place as the actuators. The exact positions of the actuator, gaussmeter probe and the magnet (distance d away from the actuator) were used in the simulations. B. Magnetic flux density recorded at the position of the probe as a function of the normal distance d was obtained from a 3D simulation of the $2'' \times 2'' \times 0.5''$ magnet analogous to results in fig. S13C.

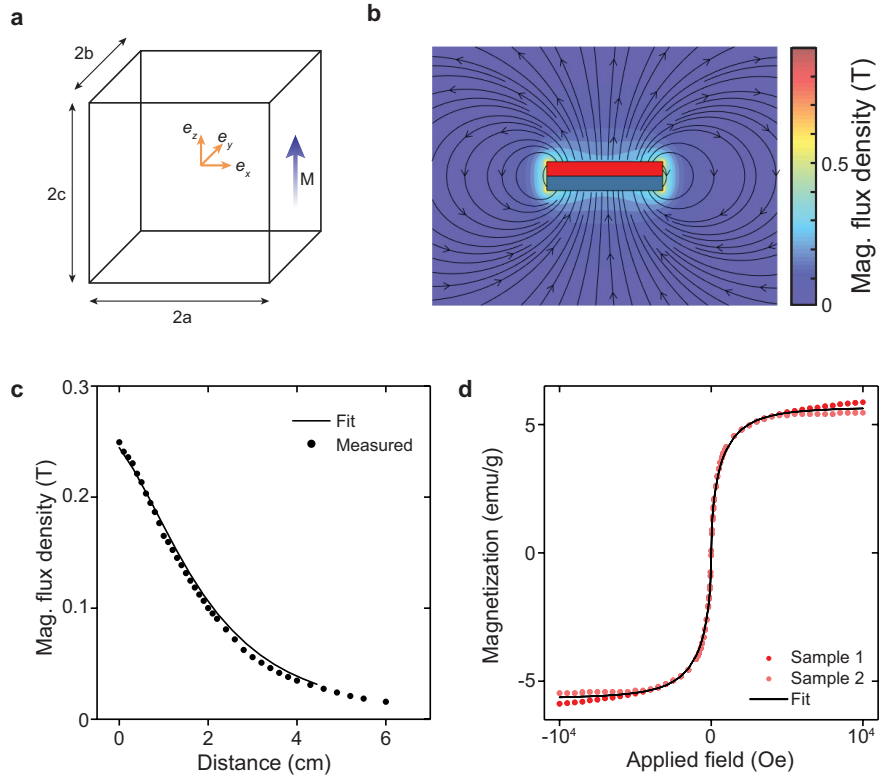


Fig. S13. Modeling of the external magnetic field. A. Schematic representation of a permanent magnet vertically magnetized (see Methods for magnetic field computation using this coordinate system). B. Magnetic flux density analytically computed corresponding to a $2'' \times 2'' \times 0.5''$ magnet with a magnetic moment of 950 kA/m . C. Measured and fitted magnetic flux densities corresponding to the above magnet (as a function of distance from the the magnet measured along the central axis). D. Measured MPC magnetization curves.

Movie S1. Video showing the dynamic actuation of the reflective panel array used to raster the MIT logo. The electromagnet used to generate the magnetic field is powered by a current source, with the current manually varied between 0 A and 7.5 A.

Movie S2. The printed water lily is placed at fluid interfaces and actuated using a permanent magnet. The video shows results of experiments performed at the silicone oil-water interface.

Movie S3. Actuation of panel actuators at different frequencies for bandwidth measurements and long-term actuation (1000 cycles).

Movie S4. Topology optimization of actuators. The video shows results from two examples of topology optimized actuators, i. “Van Gogh” – “Scream” and ii. 3×3 array of the “Grass” – “Stones” design. For each example, the ray-traced front view and tilted view of the topology optimized design is shown over the course of the iterations. Finally, the experimental results of the printed actuators are shown.